energies

MDPI

Article

Effects of Organ-Pipe Chamber Geometry on the Frequency and Erosion Characteristics of the Self-Excited Cavitating Waterjet

Tengfei Cai [1,2], Yan Pan [1], Fei Ma [1,*] and Pingping Xu [1]

[1] School of Mechanical Engineering, University of Science and Technology Beijing, Beijing 100083, China; caitengfei92@163.com (T.C.); panyan_petra@126.com (Y.P.); xpp919@imust.cn (P.X.)
[2] Department of Mechanical Science and Engineering, University of Illinois at Urbana-Champaign, Urbana, IL 61801, USA
* Correspondence: yeke@ustb.edu.cn

Received: 20 January 2020; Accepted: 17 February 2020; Published: 21 February 2020



Abstract: Erosion experiments were performed to uncover the impact of organ-pipe chamber geometry on the frequency and erosion characteristics of self-excited cavitating waterjets. Jets emanating from self-excited nozzles with various organ-pipe geometries were investigated. The upstream and downstream contraction ratios of the organ-pipe resonator were changed respectively from 1.5 to 6 and 2 to 12. Pressure sensors and hydrophone were used to characterize jets' frequency characteristics. Mass loss was also obtained in each of the configurations to assess the erosion performance. By tuning the self-excited frequency, the peak resonance was achieved using the nozzles with different geometries. Accordingly, the acoustic natural frequencies of various chamber geometries were obtained precisely. Results show that with increasing upstream and downstream contraction ratio of the organ-pipe chamber, the acoustic natural frequency increases monotonically due to the reduction of equivalent length, while the resonance amplitude and mass loss first increase and then decrease. There are optimum geometric parameters to reach the largest resonance amplitude and erosion mass loss: the upstream contraction ratio being between two and four, and downstream ratio being between four and seven. The effective length of the organ pipe can be calculated by the sum of the physical length and equivalent length to accurately obtain the acoustic natural frequency. Under the optimized parameters, the equivalent length can be estimated as $0.35D$.

Keywords: organ pipe; frequency characteristic; self-excited waterjet; erosion; cavitating

1. Introduction

Waterjet technology as a non-conventional processing method is widely used in mining [1,2], cleaning [3], rock breaking [4] and cutting [5]. Nevertheless, the high energy consumption and low efficiency of the traditional waterjet limited its application. To make better use of waterjet technology and lower its energy consumption, various kinds of waterjets have been invented, such as the pulsed waterjet [6,7], abrasive waterjet [8], cavitating waterjet [9,10], and so on. As environmentally friendly technologies, the pulsed waterjet can take advantage of the water hammer effect [11], and the cavitating waterjet can harvest the energy of cavity collapse [9,12]; both of them can significantly lower the energy consumption during the working process. It is noteworthy that a self-excited cavitating waterjet, which combines the superiority of pulsed and cavitating waterjets, can produce strong pressure oscillation and intensive cavitation erosion [13]. Thus, the self-excited cavitating waterjet has received a great deal of attention in the past decades since it was first proposed [14]. The principal self-excited configurations used to produce the self-excited cavitating waterjet include "organ-pipe nozzle", "pulser", "pulser-fed",

and "laid-back pulser" [14]. Among them, the organ-pipe nozzle has been the subject of extensive study and development due to the simple structure, low flow resistance, and strong erosion ability [15–17].

The organ-pipe nozzle is characterized by the acoustic resonant chamber, and the peak resonance will occur once the self-excited frequency (induced by vortex shedding) is close to the acoustic natural frequency of the organ pipe [18]. The self-excited frequency can be calculated by Strouhal number under specific operating condition and nozzle orifice diameter [14]. A model to estimate the self-excited frequency under various cavitation value [19] and nozzle lip geometries [20] was introduced previously. For the acoustic natural frequency, empirical acoustic analysis and experimentation done by Chahine et al. [21], which led to an approximation method to estimate the acoustic natural frequency. Recently, the effects of downstream contraction ratio [22], feeding pipe diameter [16] and area discontinuity of organ-pipe chamber [23] on the characteristics of self-excited jet were experimentally studied, which helped design the organ-pipe nozzle more optimally.

However, the specific acoustic natural frequency relies on the upstream and downstream contraction ratio of the organ pipe [24]. It is hard to obtain the exactly acoustic natural frequency from the empirical formula. Moreover, recently few studies [22,23] have focused on the resonating frequency or erosion characteristics of the self-excited waterjet produced by various organ-pipe chamber geometries. From the operational principle of the organ-pipe nozzle, it is necessary for an optimized nozzle design to obtain the acoustic natural frequency accurately and uncover the jet's frequency characteristic with different organ-pipe chamber geometries. Further more, detailed insight into the effects of chamber geometry on the erosion performance is essential to maximize a jet's efficiency.

To obtain the acoustic natural frequency of organ-pipe chamber accurately, an experimental method was proposed to obtain the acoustic natural frequency of organ-pipe chamber accurately. Additionally, the frequency and erosion characteristics of self-excited waterjet from various organ-pipe chambers with different downstream and upstream contraction ratios were studied. The details of the experimental setup and nozzle configurations are described in Section 2; the results and discussion are shown in Section 3; and the main conclusions are summarized in Section 4.

2. Experiment

Figure 1 shows a basic schematic of the experimental setup. Details of the configuration are described in our former publication [20,25]. The jet flow was provided by a motor-driven high-pressure pump. Working pressure of the pump can be continuously regulated from 0 to 65 MPa with a maximum flow rate of 60 L/min. Experiments were conducted with a stainless steel high-pressure cell. The high-pressure cell is a cylindrical pressure vessel with the inside dimensions of 1 m in length and 0.4 m in diameter. The standoff distance, namely the space between the specimen and the nozzle exit, can be continuously regulated from 0 to 200 mm with a precision of 0.5 mm controlled by a servo motor. The ambient pressure can be adjusted and maintained by a relief valve in the outflow from 0 to 5 MPa approximately. The pressure sensor was a Piezotronics ICP model 102B03 with a resonant frequency of 500 kHz. Furthermore, an RSH-10 hydrophone, having a practically flat response up to 100 kHz and usable frequency up to 200 kHz was used to measure the acoustic pressure. The main specifications of the pressure sensor and hydrophone are shown in Tables 1 and 2. The position of the hydrophone was set at the same height as the target plate, and the horizontal distance between the sensor and the jet was 100 mm. Both the pressure and noise signals were monitored and recorded with a sampling frequency of f_s = 204.8 kHz by the data logger (model: LMS SCADAS Mobile SCM05). Therefore, the resonance state could be observed and controlled in real-time.

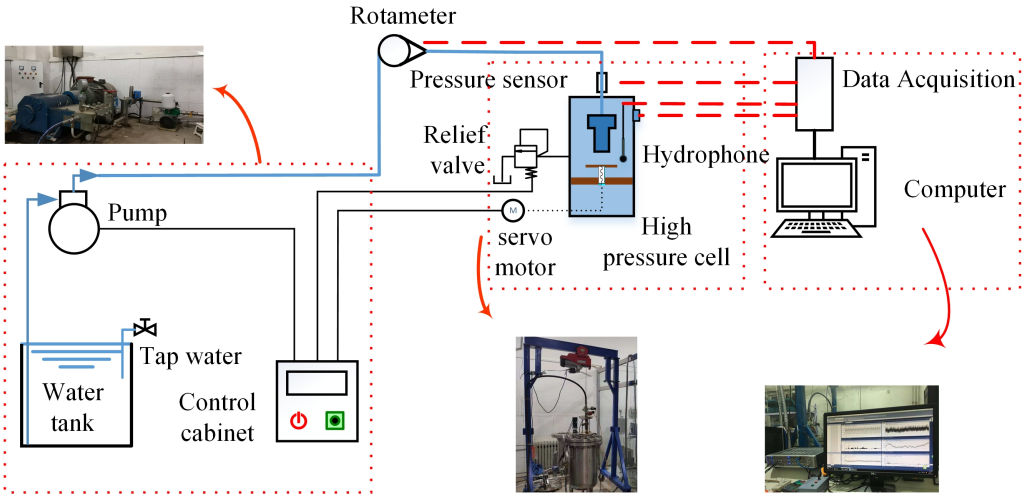


Figure 1. Schematic of the experimental setup.

Table 1. Main specifications of the pressure transducer.

Performance	Parameters
Model	102B03
Measurement Range	69 MPa
Maximum Pressure	103.42 MPa
Resonant frequency	≥500 kHz
Non-Linearity	≤1% FS

Table 2. Main specifications of the hydrophone.

Performance	Parameters
Model	RSH-10
Usable frequency range	1–200 kHz
Linear frequency range	1–100 kHz
Receiving sensitivity nominal	≥210 dB

As shown in Figure 2, the organ-pipe nozzle consists of an upstream area contraction (D_s/D); a downstream area contraction (D/d); and a resonant chamber with a length of L and a diameter of D. Peak resonance will occur when the acoustic natural frequency of the resonant chamber is close to the self-excited frequency. The fundamental of self-excited frequency f^*, induced by vortex shedding, can be defined as

$$f^* = \frac{S_d v}{d} \tag{1}$$

where, d and v are the diameter and velocity of the jet individually, and S_d is the Strouhal number.

The organ pipe's acoustic natural frequency f_n is mainly determined by the chamber length L which is expressed below [26]:

$$f_n = \frac{K_n c}{L} \tag{2}$$

For $D_s/D > 1$, the "mode parameter" K_n is given, by

$$K_n = \begin{cases} n/2, & D/d < 1/\sqrt{M}; \\ (2n-1)/4, & D/d > 1/\sqrt{M} \end{cases} \tag{3}$$

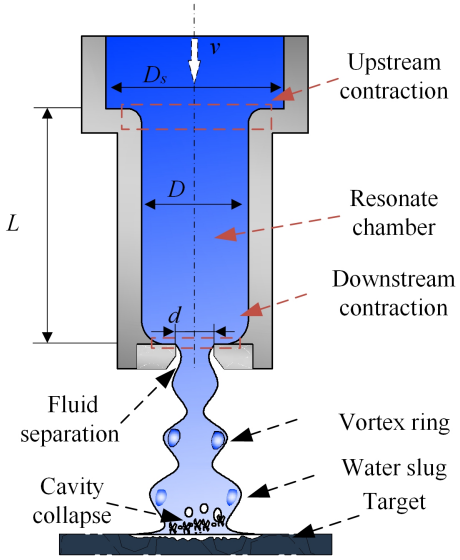


Figure 2. Schematic of the organ-pipe nozzle geometry and generation of a self-excited cavitating waterjet.

In these expressions, n is the mode number of the organ-pipe chamber, and M stands for the Mach number. When f^* approaches f_n, the resonance frequency f_r occurs and is denoted as $f_r = f^* \approx f_n$. Based on Equations (2) and (3), the acoustic natural frequency of the chamber can only be estimated roughly, because the exact f_n is dependent on the contraction at each end of the organ-pipe chamber [18]. Therefore, to uncover the influence of organ-pipe geometry on the jet's frequency characteristics, organ-pipe chamber with different upstream and downstream contraction ratio were experimentally researched at present. Geometries of the organ-pipe chamber employed are listed in Table 3.

To uncover the influence of upstream and downstream contraction ratios respectively, when changing the value of D_s/D or D/d, the other variables are consistent. In all cases, the upstream pressure is consistent. P_u = 15 MPa with normalized standoff $S = 3d - 4d$.

Table 3. Geometric parameters of the organ pipe.

D_s/D	D/d	d (mm)	L (mm)
1.5–6	5	2	24
3	2–12	2	24

A pure aluminum (1070A Chinese Industry Standard) specimen, widely used by lots of researchers [23,27], is set perpendicularly to the jet during the erosion experiments. The test surface of the specimen is lightly machined and polished to a surface roughness of 0.4 μm, to minimize surface damage or alteration. Table 4 shows the working condition, including the upstream pressure P_u, the material, the attack angle θ, the water temperature and the erosion time t. Before and after each test, the specimen is dried and reweighed by an electronic balance (JJ224BF, 0.1 mg) to determine its mass weight loss.

Table 4. Working conditions.

Name	Parameters
Upstream pressure P_u	15 MPa
Material	Aluminum
Attack angle θ	90°
Water temperature	18 °C
Erosion time t	5 min

3. Results and Discussion

3.1. Resonant Frequency Characteristics of the Self-Excited Waterjet

First, pressure signals from the transducer were investigated to illuminate the pressure fluctuation characteristics of the self-excited waterjet. Figure 3 shows the typical time-dominant pressure signals under the resonant and non-resonant conditions. A high-pass filter with a cut-off frequency of 500 Hz was used to block the low-frequency interference from the plunger pump. As shown in Figure 3, the time-domain signal helps with a visual understanding of how the jets oscillate under different conditions. Under the resonant status, the pressure fluctuates periodically and violently, and the amplitude is an order higher than that of the non-resonant status.

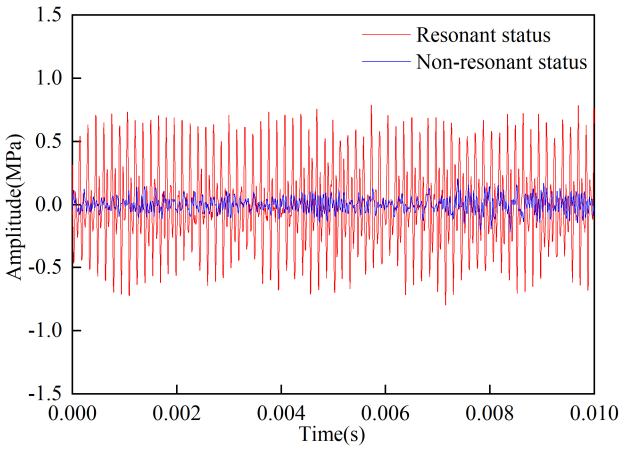


Figure 3. Time-dominant pressure fluctuation characteristics of the self-excited waterjet.

The peak resonance state is critical to investigating the influence of the organ-pipe chamber geometry. As the peak resonance will only occur in the case of match between the self-excited frequencies of the jet oscillation and the acoustic natural frequencies of the chamber, and the latter is constant for a specific chamber geometry, the study of the self-excited frequencies becomes the research emphasis. Based on Equation (1), when the jet velocity and the nozzle configuration are fixed, the self-excited frequencies are related to the Strouhal number. Accordingly, a simple relation between the Strouhal number and the cavitation number is given in previous study [19]. Therefore, in this study, the nozzle geometries are regulated to generate different acoustic natural frequencies; the cavitation number is adjusted to control the self-excited frequencies, peak resonance occurs by the adjustment and match between these conditions.

The waterfall spectra of the pressure fluctuation are shown in Figure 4a. It is clear that spectra include not only the fundamental frequency but also lots of harmonics, which agree with the result obtained by Chahine et al [28]. The fundamental self-excited frequency f^* can be confirmed by "triad-resonance" [29]. Note that all of those different frequencies increase as the cavitation number increases, along with the changing of oscillating amplitude. The exact self-excited frequency and root mean square (RMS, the square root of the arithmetic mean of the squares of the pressure fluctuation) of

the pressure fluctuation are shown in Figure 4b, both as a function of cavitation number. It is obvious that the self-excited frequency increases monotonically from 8.45 kHz to 13.2 kHz as the cavitation number changes from 0.044 to 0.15. The RMS of pressure fluctuation fluctuates significantly over the test range. As the cavitation number increases from 0.13 to 0.15, the value of RMS rises dramatically, peaking at $\sigma = 0.14$ where $f^* = 13$ kHz. From those above analysis, the self-excited waterjet reaches the peak resonance when f^* kHz is close to f_n, and the resonance frequency of the organ-pipe chamber can be confirmed as $f_r \approx 13$ kHz.

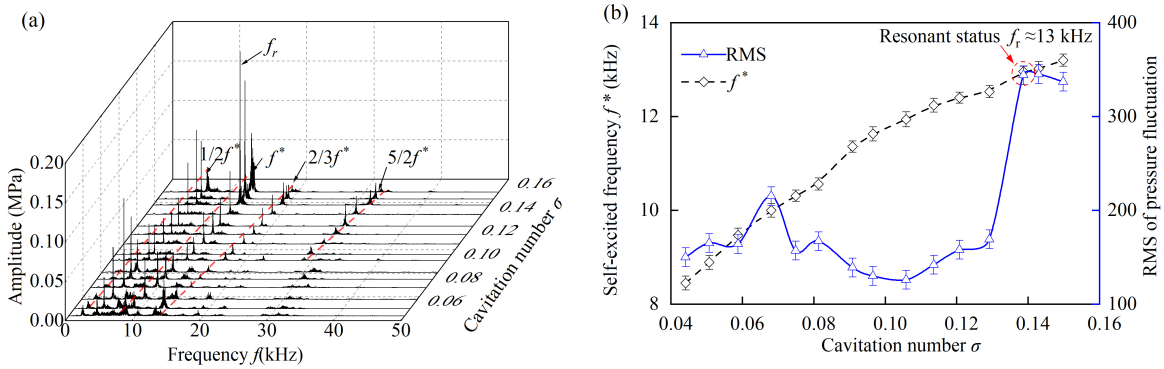


Figure 4. Different oscillation statuses of the self-excited waterjet. (**a**) Waterfall spectra of pressure fluctuation as a function of cavitation number; (**b**) frequency and pressure fluctuation RMSs as a function of cavitation number.

3.2. Frequency and Erosion Characteristics with Various Upstream Contraction Ratios

To uncover the frequency and erosion characteristics of the self-excited cavitating waterjet produced by various organ-pipe nozzles with different upstream contraction ratios, the pressure fluctuation and noise were measured simultaneously. The method proposed in Section 3.1 was used to achieve the peak resonance in each case. The erosion experiments were also completed with D_s/D in a range of 1.5–6; under each condition the standoff distance was selected for the jet to achieve strong resonance.

Figure 5a illustrates the relationship between the frequency spectra of the pressure fluctuation and the upstream contraction. The upstream contraction ratio causes a significant effect on the amplitude of the pressure fluctuations. Note that the pressure sensor is mounted on the feeding pipe right upstream of the nozzle; thus the pressure wave attenuation rate is different once the chamber geometry changes. Therefore, the resonance intensity could not be evaluated accurately by the amplitude of the pressure fluctuation alone. In a previous study [25,30], the pressure signal and the cavitation noise of the cavitating jet were obtained by the pressure sensor and the hydrophone respectively. Moreover, it was found that the dominant frequencies in the frequency spectrum of the pressure fluctuation were similar to those in the power spectrum density of the cavitation noise. Therefore, in the following section, the noise signal was also used to analyze the frequency characteristics of the self-excited waterjet.

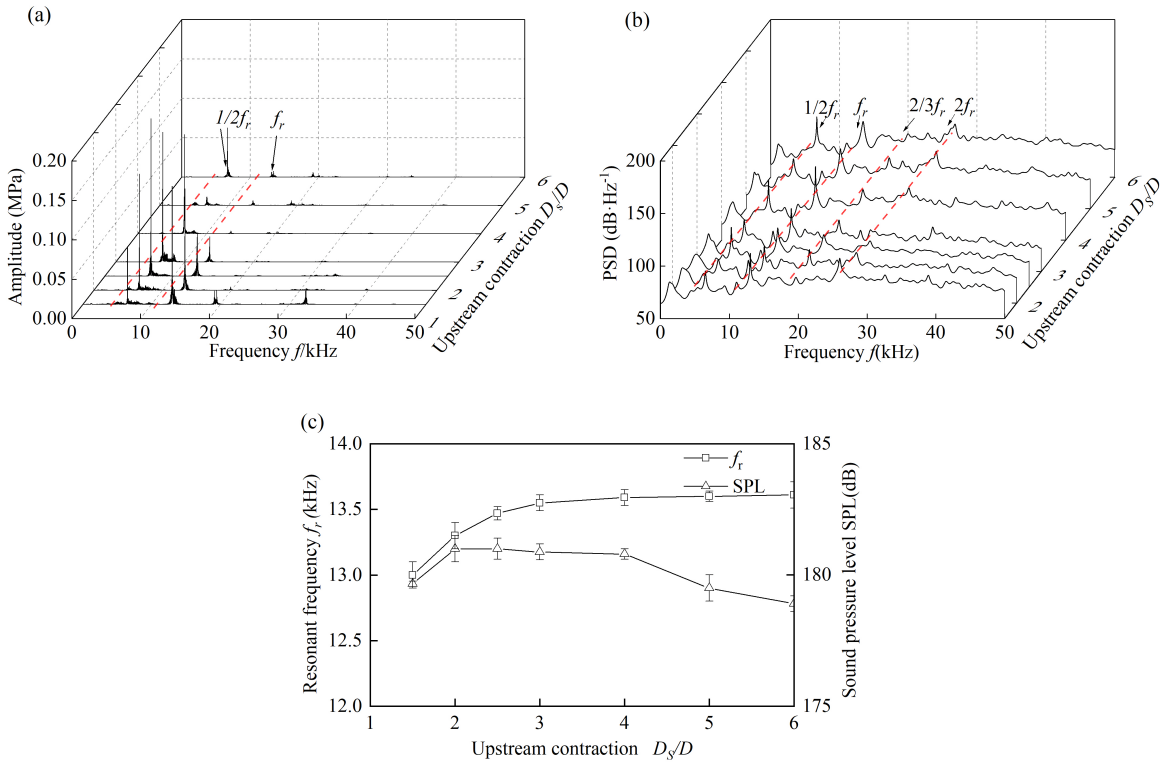


Figure 5. Frequency characteristics of self-excited waterjet as a function of upstream contraction ratio D_s/D. (**a**) Spectra of self-excited waterjet's pressure fluctuation with D_s/D from 1.5 to 6; (**b**) power spectrum density of self-excited waterjet's noise with D_s/D from 1.5 to 6; (**c**) resonance frequency and sound pressure level (SPL) as a function of upstream contraction ratio D_s/D.

Figure 5b illustrates the PSD (power spectral density) of the self-excited waterjet's noise produced by the nozzles with different upstream contraction ratios. The spectra of pressure and noise signals show a similar structure(Figure 5a,b). Most of them include the fundamental resonant frequency and its harmonics. It can be seen that the fundamental frequency and its harmonics increase slightly with the upstream contraction. To quantitatively evaluate the effect of the upstream contraction ratio, as shown in Figure 5b, the variation of the resonance frequency and the sound pressure are revealed. As D_s/D increases from 1.5 to 6, the f_r increases from 13 kHz to 13.6 kHz monotonously at first and remains stable at 13.6 kHz after $D_s/D > 3$. Meanwhile, the sound pressure level (SPL) rises dramatically and reaches its peak at $D_s/D = 2$. After that, the SPL remains steady at 181 dB when $2 < D_s/D < 4$ and declines gradually after $D_s/D = 4$. A similar result also was reported by Black: that large D_s could improve the acoustic resonance [30]. The chamber geometry can change the pressure oscillation amplitude, and, in turn, can affect the cavitation development process. As a result, the SPL of noise produced by pressure oscillation and cavitation noise also is changed significantly as upstream contraction ratio.

As shown in Figure 6, the variation of the mass loss and the macroscopic appearances under different upstream contraction ratios are revealed. It is clear that the mass loss shows a similar trend with SPL. The mass loss peaks at $D_s/D = 2.5$, and is larger than 0.02 mg when $2 < D_s/D < 4$. The erosion depth of $D_s/D = 2.5$ is deeper than that of $D_s/D = 1.5$, which can account for the larger mass loss of the former. Details will be discussed later in Section 3.4.

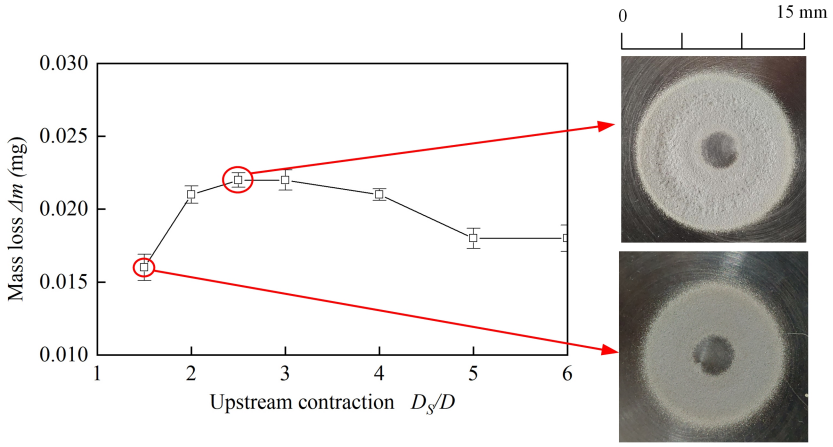


Figure 6. Mass loss and macroscopic appearance as a function of upstream contraction ratio D_s/D.

3.3. Frequency and Erosion Characteristics with Various Downstream Contraction Ratios

In this section, the influences of organ-pipe chamber downstream contraction ratio on the frequency and erosion characteristics of the self-excited cavitating waterjet are characterized. As shown in Figure 5c, the resonance intensity reach its peak during $2 < D_s/D < 4$. Therefore, D_s/D is fixed at three as the downstream contraction ratio is varied in a range of 2–12.

The frequency characteristics of self-excited waterjet as a function of downstream contraction ratio D/d are shown in Figure 7. The amplitude of the pressure fluctuation spectra increases and then decreases as D/d increases from 2 to 12. Moreover, the amplitude of pressure fluctuation is also affected by the pressure wave attenuation under various chamber geometries. As a result, the power spectrum density of noise with different downstream contraction ratios was illustrated in Figure 7b. It is clear that the spectrum structure is similar to Figure 5b. The resonance frequency and sound pressure level as a function of the D/d are given in Figure 7c to evaluate the effects quantitatively. As shown in Figure 7c, the resonance frequency fluctuates around 13.4 kHz as D/d increases from 2 to 9.

As shown in Figure 7, the frequency property of the self-excited waterjet under different downstream contraction ratio D/d is given. With the increase of D/d in a range of 2–12, the amplitude of the pressure fluctuation rises first and descends later. Additionally, the pressure fluctuation is affected by the pressure wave attenuation under various chamber geometries. The PSD of the cavitation noise is shown in Figure 7b, and the frequency structure is similar with that in Figure 5b. As shown in Figure 7b, the effect of the downstream contraction ratio is evaluated quantitatively. During the variation of D/d in a range of 2–9, the resonance frequency fluctuates around 13.4 kHz. After that, the frequency rises dramatically from 13.4 kHz to 13.8 kHz. It is noteworthy that the mode parameter $K_n = 1/4$ and does not change within the experimental range of D/d. The SPL rises monotonically as D/d increases from 2 to 5, and remains at 181 dB when D/d ranges within 5–9.

To illustrate the erosion characteristic evolution as the increase of D/d, the mass loss and the macroscopic appearance under different D/d are shown in Figure 8. The mass loss rises as the D/d increases from two to four, and decreases gradually as D/d exceeds seven. The mass loss peaks at $D/d = 4$ and fluctuates around $\Delta m = 0.02$ mg. The macroscopic appearance also shows significant differences that the erosion area at the case of $D/d = 7$ is two times of $D/d = 2$. Note that the diameter of the slightly eroded center is bigger under smaller D/d, which indicates the different shape of the cavitation cloud.

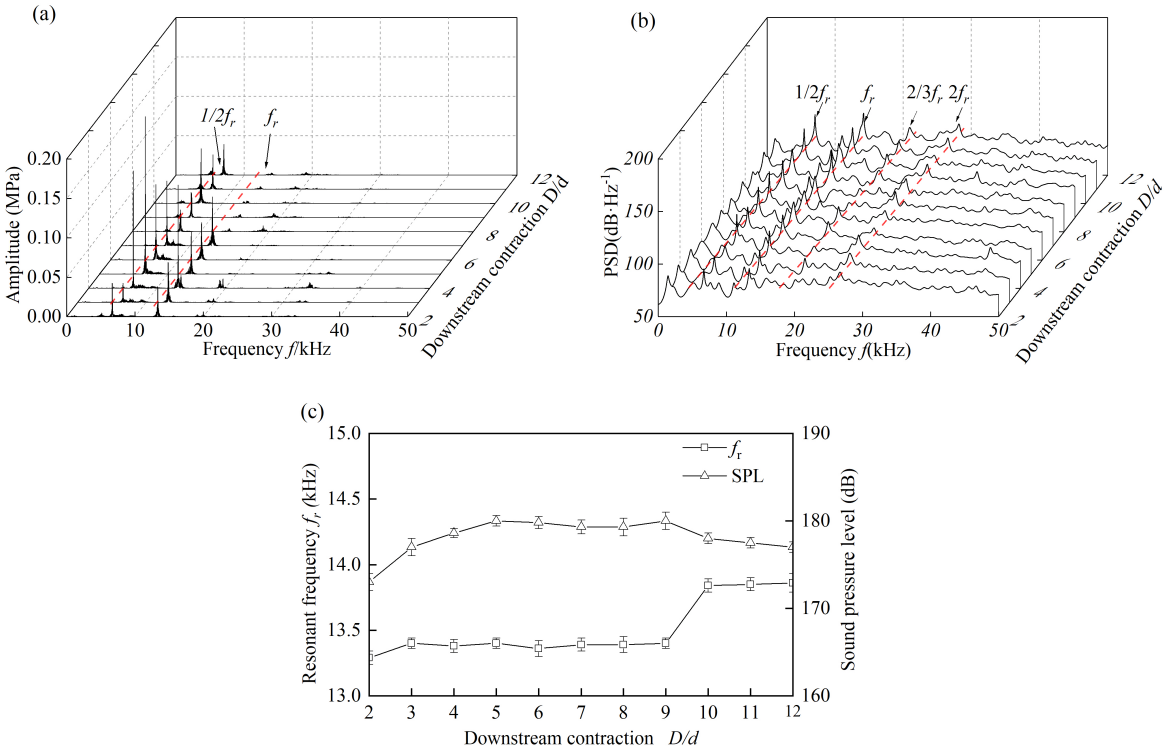


Figure 7. Frequency characteristics of self-excited waterjet as a function of downstream contraction ratio D/d. (**a**) Spectra of self-excited waterjet's pressure fluctuation with D/d from 2 to 12; (**b**) power spectrum density of self-excited waterjet's noise with D/d from 2 to 12; (**c**) resonance frequency and SPL as a function of downstream contraction ratio D/d.

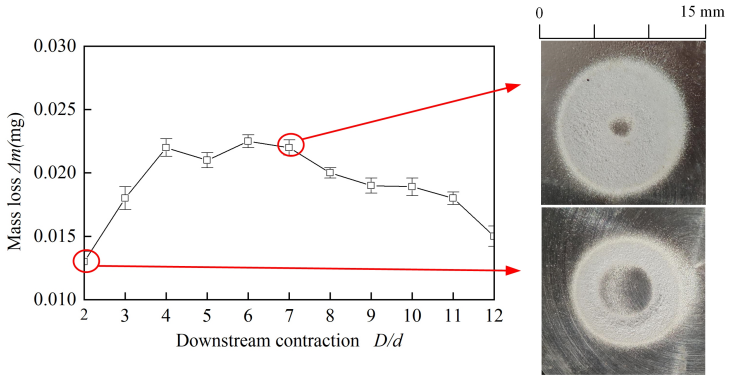


Figure 8. Mass loss and macroscopic appearance as a function of downstream contraction ratio D/d.

3.4. Discussion

The influences of organ-pipe chamber geometry to the frequency and erosion characteristics of the self-excited cavitating waterjet were preliminarily revealed in the above section. Now, the effect mechanism will be discussed from the view of acoustic resonance and cavitation mechanism.

Based the Equations (2) and (3), to achieve $f_r = f^* \approx f_n$, the mode parameter K_n is equal to $1/4$ when $2 < D/d < 12$. In those experiments, the upstream pressure P_u = 15 MPa, the velocity and Mach number can be calculated by the Bernoulli principle ($M \approx 0.115$). During the test process, the value of D/d is larger than $\sqrt{M}$, which can be used to account for the mode of the natural frequency. The research done by Johnson et al. [24] found that only when $(D/d)^2 \approx 1$ could the mode parameter be selected as $n/2$. From Figure 6b, with $4 < D/d < 9$, the resonance intensity reaches the peak, so the mode parameter should be set as $(2n-1)/4$ for most conditions.

Based on the analysis above, the organ-pipe chamber tested in this experiment can be regarded as a quarter-wave resonator, whose conceptual schematic is shown in Figure 9. In the upstream contraction area, the upstream impedance Z_u is assumed to be zero, but this is not the case. The condition at the upstream area is not $Z_u = 0$ because the open end of the pipe radiates sound into the surrounding medium. According to the values of particular impedance for different end conditions, the equivalent extension tube ΔL_1 is about $0.3D$ to $0.42D$ for an unflanged or infinite flange pipe [31]. As for the downstream contraction area, the downstream impedance Z_d also is not infinite due to the existence of the hole. Therefore, there is also another equivalent extension tube ΔL_2 at the end of the tube. So the effective length of the organ pipe is

$$L_e = L + \Delta L \tag{4}$$

As shown in Figure 9, the equivalent extension is contributed by both upstream contraction and the downstream contraction.

$$\Delta L = \Delta L_1 + \Delta L_2 \tag{5}$$

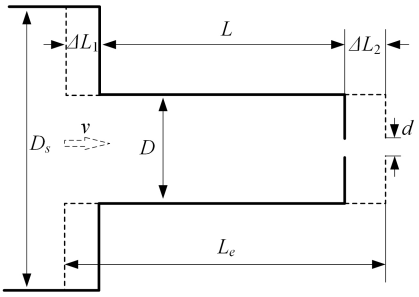


Figure 9. Conceptual schematic of the organ-pipe chamber's effective length.

Based on the Equations (2)–(4), and Figures 5c and 6c, the relationship between the equivalent extension, the upstream contraction ratio and the downstream contraction radio is given in Figure 10. As upstream contraction increases, the equivalent extension decreases inversely (Figure 10a) and the value of ΔL gets close to 3.5 mm; namely, 0.35D. The experimental results are in an agreement with previous studies, where most of the contribution comes from ΔL [31]. It can be seen in Figure 10b that the ΔL fluctuates around 4 mm until $D/d > 9$. Even the ΔL shortens sharply when $D/d > 9$; it is out of the optimal range to reach the intense resonance. As a result, for a quarter-wave organ-pipe resonator, within a range of the optimal geometric parameters, the equivalent extension ΔL could be chosen as $0.35D$ to $0.4D$.

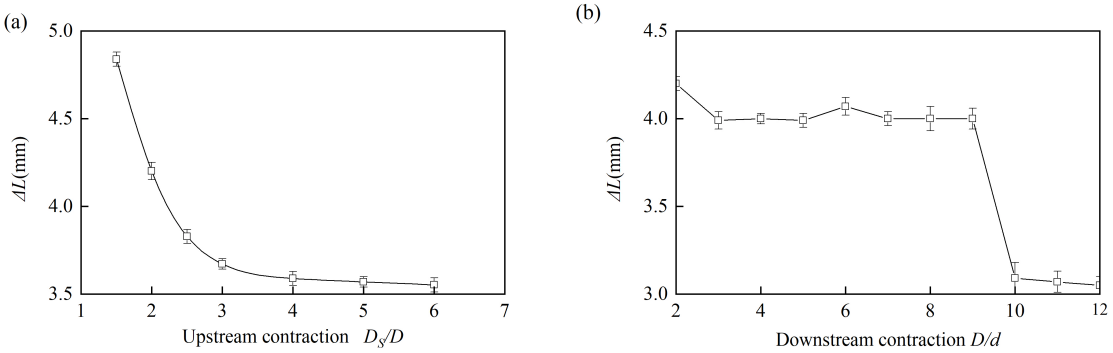


Figure 10. Equivalent extension length ΔL as a function of upstream and downstream contraction ratio. (**a**) ΔL as a function of upstream contraction ratio D_s/D; (**b**) ΔL as a function of downstream contraction ratio D/d.

The intense pressure oscillations of the self-excited cavitating waterjet can induce strong cavitation and reduce the water cushion effect, which can significantly improve jet erosion performance. Therefore, the organ-pipe chamber geometries including upstream and downstream contraction ratios, can influence a jet's erosion performance by changing the pressure oscillation amplitude. The erosion mass loss achieves its peak value at a similar range to sound pressure level, which is consistent with the above inference. It is noteworthy that the erosion characteristic also could be impacted by the fluid behavior. In cases with different downstream contraction ratios (e.g., the increase of D/d), the enhanced fluid separation (as shown in Figure 2) promotes the formation of cavitation, which could account for the different appearance in Figure 8. However, there is a balance between enhancing cavitation and hydraulic loss, so the erosion performance decreases when D/d is too large.

4. Conclusions

In this study, the effects of organ-pipe chamber geometry on the frequency and erosion characteristics were characterized by analyzing the pressure signals and mass loss during the erosion experiments. By changing the self-excited frequency to achieve the peak resonance, the resonance frequencies of various organ-pipe chambers were obtained precisely to uncover its frequency characteristic. The general tendency is the resonate frequency increases monotonically with increasing upstream and downstream contraction ratios due to the reduction of equivalent length. The resonance amplitude and erosion ability first increase and then decrease with increasing contraction ratios. The optimum geometric parameters to reach the largest resonance amplitude and mass loss are: upstream contraction ratio D_s/D = 2–4 and, downstream ratio D/d = 4–7. To obtain organ-pipe chamber's acoustic natural frequency, its effective length is the sum of its physical length and equivalent length. Combining the experimental results and acoustic theory, the equivalent length can be estimated as $0.35D$ under the above optimized parameters. The above results can provide a basis for the optimized design of the self-excited nozzle, so as to significantly improve the efficiency and reduce energy consumption in the industrial cleaning and cutting under submerged condition.

Author Contributions: Conceptualization, T.C.; formal analysis, T.C. and P.X.; writing—review and editing, T.C. and Y.P.; supervision, F.M. All authors have read and agreed to the published version of the manuscript.

Funding: This work is supported by the National Natural Science Foundation of China (No. 51774019), the Ministry of Science and Technology of the People's Republic of China (No. 2016YFC0802900), and the China Scholarship Council (No. 201806460056).

Conflicts of Interest: The authors declare no conflict of interest.

References

1. Fang, Z.; Wu, Q.; Zhang, M.; Liu, H.; Jiang, P.; Li, D. Large Eddy Simulation of Self-Excited Oscillation Pulsed Jet (SEOPJ) Induced by a Helmholtz Oscillator in Underground Mining. *Energies* **2019**, *12*, 2161. [CrossRef]
2. Liu, C.; Xia, B.; Lu, Y. Coalbed Methane Extraction Using the Self-Oscillating Water Jet Slotting Method. *Energies* **2018**, *11*, 897. [CrossRef]
3. Careddu, N.; Akkoyun, O. An investigation on the efficiency of water-jet technology for graffiti cleaning. *J. Cult. Herit.* **2016**, *19*, 426–434. [CrossRef]
4. Tripathi, R.; Hloch, S.; Chattopadhyaya, S.; Klichová, D.; Ščučka, J.; Das, A.K. Application of the pulsating and continous water jet for granite erosion. *Int. J. Rock Mech. Min. Sci.* **2020**, *126*, 104209. [CrossRef]
5. Shanmugam, D.; Masood, S. An investigation on kerf characteristics in abrasive waterjet cutting of layered composites. *J. Mater. Process. Technol.* **2009**, *209*, 3887–3893. [CrossRef]
6. Raj, P.; Hloch, S.; Tripathi, R.; Srivastava, M.; Nag, A.; Klichová, D.; Klich, J.; Hromasová, M.; Muller, M.; Miloslav, L.; et al. Investigation of sandstone erosion by continuous and pulsed water jets. *J. Manuf. Process.* **2019**, *42*, 121–130. [CrossRef]
7. Foldyna, J.; Sitek, L.; Švehla, B.; Švehla, Š. Utilization of ultrasound to enhance high-speed water jet effects. *Ultrason. Sonochem.* **2004**, *11*, 131–137. [CrossRef]

8. Selvam, R.; Karunamoorthy, L.; Arunkumar, N. Investigation on performance of abrasive water jet in machining hybrid composites. *Mater. Manuf. Process.* **2017**, *32*, 700–706. [CrossRef]
9. Soyama, H. Key factors and applications of cavitation peening. *Int. J. Peen. Sci. Technol.* **2017**, *1*, 3–60.
10. Conn, A.F.; Johnson, V., Jr.; Liu, H.; Frederick, G. *Evaluation of CAVIJET Cavitating Jets for Deep-Hole Rock Cutting*; Technical Report; Hydronautics, Inc.: Laurel, MD, USA, 1981.
11. Hloch, S.; Adamčík, P.; Nag, A.; Srivastava, M.; Čuha, D.; Müller, M.; Hromasová, M.; Klich, J. Hydrodynamic ductile erosion of aluminium by a pulsed water jet moving in an inclined trajectory. *Wear* **2019**, *428*, 178–192. [CrossRef]
12. Ball, C.; Fellouah, H.; Pollard, A. The flow field in turbulent round free jets. *Prog. Aerosp. Sci.* **2012**, *50*, 1–26. [CrossRef]
13. Li, D.; Wang, Z.; Yuan, M.; Fan, Q.; Wang, X. Effects of Nozzle Exit Angle on the Pressure Characteristics of SRWJs Used for Deep-Hole Drilling. *Appl. Sci.* **2019**, *9*, 155. [CrossRef]
14. Johnson, V., Jr.; Lindenmuth, W.; Conn, A.; Frederick, G. *Feasibility Study of Tuned-Resonator, Pulsating Cavitating Water Jet for Deep-Hole Drilling*; Technical Report; Sandia National Labs.: Albuquerque, NM, USA; Hydronautics, Inc.: Laurel, MD, USA, 1981.
15. Chahine, G. Mechanics and application of self-resonating cavitating jets. In Proceedings of the International Symposium on Jets & Cavities, Miami Beach, FL, USA, 17–22 Novermber 1985; pp. 21–33.
16. Li, D.; Kang, Y.; Ding, X.; Liu, W. Experimental study on the effects of feeding pipe diameter on the cavitation erosion performance of self-resonating cavitating waterjet. *Exp. Therm Fluid Sci.* **2017**, *82*, 314–325. [CrossRef]
17. Gensheng, L.; Zhonghou, S.; Changshan, Z.; Debin, Z.; Hongbing, C. Investigation and application of self-resonating cavitating water jet in petroleum engineering. *Pet. Sci. Technol.* **2005**, *23*, 1–15. [CrossRef]
18. Chahine, G.L.; Johnson Jr, V.E.; Lindenmuth, W.T.; Frederick, G.S. The use of self-resonating cavitating water jets for underwater sound generation. *J. Acoust. Soc. Am.* **1985**, *77*, 113–126. [CrossRef]
19. Pan, Y.; Cai, T.; Ma, F.; Qiu, L.; Cui, L. Self-excited Frequency Estimation Model of Organ-pipe Waterjet under Confining Pressure. *J. Mech. Eng.* **2018**, *54*, 220–225. (In Chinese) [CrossRef]
20. Cai, T.; Liu, B.; Ma, F.; Pan, Y. Influence of nozzle lip geometry on the Strouhal number of self-excited waterjet. *Exp. Therm Fluid Sci.* **2020**, *112*, 109978. [CrossRef]
21. Chahine, G.; Genoux, P.F.; Johnson, V., Jr.; Frederick, G. *Analytical and Experimental Study of the Acoustics and the Flow Field Characteristics of Cavitating Self-Resonating Water Jets*; Technical Report; Tracor Hydronautics, Inc.: Laurel, MD, USA, 1984.
22. Wang, X.; Kang, Y.; Zhang, M.; Yuan, M.; Li, D. The Effects of the Downstream Contraction Ratio of Organ-Pipe Nozzle on the Pressure Oscillations of Self-Resonating Waterjets. *Energies* **2018**, *11*, 3137. [CrossRef]
23. Li, D.; Kang, Y.; Ding, X.; Wang, X.; Fang, Z. Effects of area discontinuity at nozzle inlet on the characteristics of self-resonating cavitating waterjet. *Chin. J. Mech. Eng.* **2016**, *29*, 813–824. [CrossRef]
24. Johnson, V.; Chahine, G.; Lindenmuth, W.; Conn, A.; Frederick, G.; Giacchino, G. Cavitating and structured jets for mechanical bits to increase drilling rate Part I: Theory and concepts. *J. Energy Res. Technol.* **1984**, *106*, 282–288. [CrossRef]
25. Cai, T.; Pan, Y.; Ma, F.; Cui, L.; Qiu, L. Detection method of the self-resonating waterjet characteristic based on the flow signal in a pipeline. *Chin. J. Eng.* **2019**, *41*, 377–383.
26. Johnson, V.E., Jr.; Lindenmuth, W.T.; Chahine, G.L.; Conn, A.F.; Frederick, G.S. *Research and Development of Improved Cavitating Jets for Deep-hole Drilling*; Technical Report; Hydronautics, Inc.: Laurel, MD, USA, 1984.
27. Soyama, H. Effect of nozzle geometry on a standard cavitation erosion test using a cavitating jet. *Wear* **2013**, *297*, 895–902. [CrossRef]
28. Chahine, G.L.; Johnson, V.E., Jr.; Frederick, G.S. *Self Resonating Pulsed Water Jets for Aircraft Coating Removal: Feasibility Study*; Technical Report; HYDRONAUTICS INC.: Laurel, MD, USA, 1982.
29. Petersen, R.; Clough, R. The influence of higher harmonics on vortex pairing in an axisymmetric mixing layer. *J. Fluid Mech.* **1992**, *239*, 81–98. [CrossRef]

30. Black, A.; Chahine, G.; Raymond, D.W.; Matthews, O.; Grossman, J.W.; Bertagnolli, K.U.; Vail, M.U. *Development and Testing of a Mudjet-Augmented PDC Bit*; Technical Report; Sandia National Laboratories: Albuquerque, NM, USA, 2006.
31. Kinsler, L.E.; Frey, A.R.; Coppens, A.B.; Sanders, J.V. *Fundamentals of Acoustics*, 4th ed.; Lawrence, E.K., Austin, R.F., Alan, B.C., James, V.S., Eds.; Wiley-VCH: Hoboken, NJ, USA, 1999; p. 560, ISBN 0-471-84789-5.



© 2020 by the authors. Licensee MDPI, Basel, Switzerland. This article is an open access article distributed under the terms and conditions of the Creative Commons Attribution (CC BY) license (http://creativecommons.org/licenses/by/4.0/).